ORBITAL POPULATION AND TOPOLOGY OF MG DIHYDRIDE

Ney J. Luiggi A

Grupo Física de Metales. Departamento de Física. Núcleo de Sucre. Universidad de Oriente, 6101. Cumaná. Venezuela.

** e-mail: nluiggi51@gmail.com; nluiggi@udo.edu.ve*

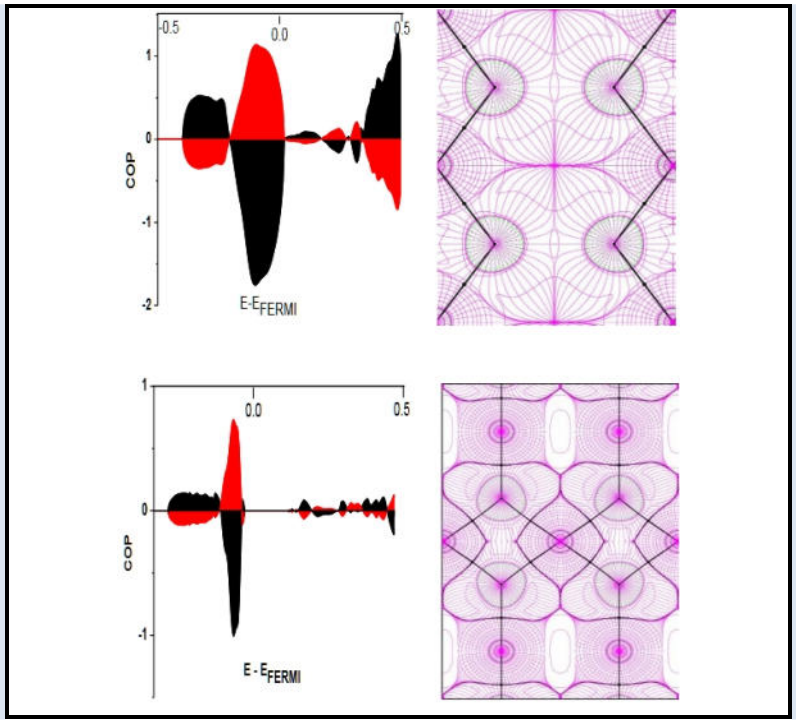

ABSTRACT

Resorting to *ab initio* methods to theoretically study the properties of materials provides a suitable avenue to delve into spaces not accessible to experimental techniques. Their benefits hinge on the precise selection of the electron charge density, which, together with a suitable Hamiltonian representing the system, provides access to each property of interest in the material. Using CRYSTAL17 software and polarization-quality double and triple zeta valence Gaussian basis sets, we performed an extensive study of the properties of Mg dihydride in its α and β structural states at zero pressure, highlighting that both hydrides are elastically stable and ductile, α-MgH_2 exhibiting a semiconducting behavior and β-MgH_2 showing a conducting character. The study of the orbital population revealed an Mg-H and Mg-Mg bonding state and an H-H anti-bonding one, the integrated population, ICOOP, showing a higher order bond in the cubic than in the tetragonal structure; and ICOHP exhibiting the β-MgH_2 hydride as more unstable than α-MgH_2. The charge density topology reflected Mg-H and H-H bond lengths little affected by the basis sets used, while their Laplacian topology revealed a region of charge concentration around Mg and a region of depletion around hydrogen and other critical points encountered, further revealing the ionic-covalente transition bond character for both structures.

Palabras Claves: Mg hydrides, topological characteristics, Bader theory, CRYSTAL software, ab initio DFT

Recibido: 22-06-2024 ; **Revisado:** 25-09-2025
Aceptado: 31-07-2025 ; **Publicado:** 30-10-2025
https://doi.org/10.5281/zenodo.18250363

pISSN: 0255-6952 | eISSN: 2244-7113
Rev. LatinAm. Metal. Mat. 2023; **43** (2): 95-115

POBLACIÓN ORBITAL Y TOPOLOGÍA DEL DIHIDRURO DE MAGNESIO

RESUMEN

El estudio teórico de las propiedades en materiales encuentra en los métodos ab-initio una poderosa herramienta para hurgar en espacios donde aún las técnicas experimentales no permiten acceder. La bondad de estos métodos depende de la precisa selección de la densidad de carga electrónica, observable físico dependiente de la función de onda, la cual junto con un adecuado Hamiltoniano representativo del sistema, da acceso a cada propiedad de interés en el material. Utilizando el software CRYSTAL17 y conjuntos de bases gaussianas de doble y triple zeta valencia con calidad de polarización, se ha realizado un amplio estudio de las propiedades del dihidruro de Mg en sus estados estructurales α y β a presión cero, destacando que ambos hidruros son elásticamente estables y dúctiles, exhibiendo el α-MgH_2 un comportamiento semiconductor y β-MgH_2 mostrando un carácter conductor. El estudio de la población orbital reveló un estado de enlace Mg-H y Mg-Mg y un estado de anti enlace H-H. La población integrada, ICOOP, muestra un orden de enlace más alto en la estructura cúbica que en la tetragonal; ICOHP muestra al hidruro β-MgH_2 más inestable que el α-MgH_2. La topología de la densidad de carga refleja longitudes de enlace Mg-H y H-H poco afectadas por los conjuntos de bases utilizados, mientras que la topología del Laplaciano de la densidad de carga reveló una región de concentración de carga alrededor de Mg y una región de agotamiento alrededor del hidrógeno y otros puntos críticos encontrados, verificando adicionalmente el carácter de enlace de transición iónico-covalente de ambas estructuras.

Palabras clave: *Aleaciones Al-Si, aleaciones mecánicas, solubilidad, microestructura, resistividad.*

1. INTRODUCCIÓN

Magnesium hydride can be obtained by several methods, primarily through the direct hydrogenation of magnesium metal at high pressure and temperature. It can also be obtained by decomposing complex hydrides using catalytic techniques or by hydrogenating already synthesized hydrides a second time to achieve a high degree of purity.

Solid hydrides are notable for their ability to store hydrogen (up to 7.66 wt % hydrogen in MgH_2) [1-7], providing clean energy. However, not all hydride storage systems are cost-effective due to the restrictions that certain H-Metal interactions impose on the dehydrogenation kinetics [8], as external energies are required for hydrogen release. In this context, theoretical experimentation or simulation has made it possible to determine characteristics in these materials that might be difficult to find out by laboratory experimentation.

Quantum mechanics establishes the basis for modeling the electronic behavior of a material by determining the charge density of crystallographic systems in equilibrium [9], *ab initio* density functional theory (DFT) being the fine-tuning tool of all that theoretical assembly. The literature [9] is aflush with many electronic models defined around the wave function and the interaction potential, and the more accurately copied the physicochemical conditions of these models, the better the results of the properties to be evaluated. Unfortunately, the universality of a model is far from being achieved because of the number of details that each property and each material possesses.

In a recent work using DFT and the cellular FLAPW method version 2018 (Full Linearized Augmented Plane Waves and muffin-tin potential), Luiggi [10] studied the structural, elastic, electronic, and topological properties of these hydrides and their behavior under the effect of pressure. However, much of the information about the H-Metal bonds coming from each of the scalar fields defining the Hamiltonian was not included because the paper only considered the topology of the charge density. It has been reported [11,12,13] that the topology of functions such as the Laplacian of the charge density, the electronic localization function, the potential energy density, and the kinetic energy yield comprise valuable information about the character of the bond and are essential elements in a complete characterization of the materials. Availing ourselves of the advantages CRYSTAL17 provides to evaluate the properties of the materials, we considered not only the topological analysis of the charge density but also that of scalar functions such as the Laplacian of the charge density, the potential density, ELF, and the virial density.

2. PARTE EXPERIMENTAL

2.1. Computational details

The *ab initio* package CRYSTAL17 [14] is a sophisticated DFT software that expands the crystallographic orbitals of the one-particle wave function into Bloch functions, which are defined in terms of the orbitals of the atoms under study. Using the restricted closed-shell calculation, α-MgH_2 and β-MgH_2 were studied at zero pressure within the generalized gradient approximation (GGA) approach. The Perdew *et al*. exchange-correlation functional (PBESOL) [15], a revised version of PBE [16] for solids, was used in the spin-unpolarized condition. The convergence threshold in the total energy was 10^{-7}, while the truncation criteria for the two-electron integrals were 7, 7, 7, 7, 7, 7, and 14. The basis sets selected for Mg and H atoms were the double- and triple-zeta valence Gaussian basis sets with polarization quality (Mg_pob-TZVP_rev2 and H_pob-TZVP_rev2) derived from Oliveira *et al.* [17]. We used 14 primitive GTOs for the s-symmetric species of Mg, seven GTOs for the p orbitals, and five and three contracted GTOs for the s and p orbitals, respectively, in three close s and 1 p shells, while for H, we used five primitive s and three contracted GTOs in one open shell.

In this work, all properties were evaluated at zero pressure with several K vectors in the first Brillouin zone of 1183 for the tetragonal structure (α-MgH_2) and 413 for the cubic one (β-MgH_2). TOPOND software was used to determine the Mg-H bond character and other topological aspects of charge density-dependent scalar functions.

2.2. Crystal structure of the hydrides under study

Magnesium hydride crystallizes in three different crystal structures, of which the α-MgH_2 centered tetragonal structure (with P42/2 mnm (136) symmetry) and the β-MgH_2 centred face cubic structure (with Fm3m (225) symmetry) are the most

pISSN: 0255-6952 | eISSN: 2244-7113
Rev. LatinAm. Metal. Mat. 2023; **43** (2): 95-115

stable. Their crystal parameters have been reported by several authors, in particular in the Inorganic Crystal Structure Database (ICSD) and the Materials project (mp), where they are referred to as α-MgH_2 (ICSD-168831 and mp-23710) and β-MgH_2 (ICSD-168832 and mp-1008901) respectively. While there is agreement in the space groups reported in both databases for the tetragonal hydride, this is not the case for the cubic hydride.

The experimental values of the crystalline parameters reported in these databases and by other authors serve as initial input data for the self-consistent calculations. Numerical optimization algorithms are used to obtain the final parameters. The selected electronic models, the basis set of each atom and the tolerance in the evaluation of potentials and energies are factors that influence the optimization.

Table 1 summarizes the crystalline parameters of the hydrides under investigation as reported in the literature, while Fig. 1.a and 1.b show the graphical details of the bonds between atoms involved.

Table 1. Crystal parameters of the hydrides under study

Hydride	a = b (a.u)	c (a.u)	Volume (Å^3)	Atoms/cell / Wyckoff position	Ref.
α-MgH_2	8.5057 8.4916 8.3700 8.4924 8.4660	5.6887 5.6798 5.6530 5.6786 5.6503	60.99 60.69 58.69 60.69 60.01	6 2 Mg (2a) 4 H (4f)	[18] [10] This work * **
β-MgH_2	9.0540 9.0098 8.9119 9.0631 8.9951	9.0540 9.0098 8.9119 9.0631 8.9951	108.381 108.378 104.885 110.31 107.850	12 4 Mg(4a) 12 H(8c)	[19] [10] This work * **

*Inorganic Crystal Structure Database (ICSD)[20] ** Materials project Database(mp) [21]

The initial crystal parameters of α-MgH_2 and β-MgH_2 used in this work are those reported by Luiggi [10] using WIEN2K18 after optimization. Our parameters were optimized using CRYSTAL17 (Table 1). This table shows the slight deviations introduced in the lattice parameter when different software programs were selected. The atomic coordinates and lattice parameters were optimized for each structure by resorting to the full optg command, which uses the gradient of the function as an optimization method requiring an initial estimate of the Hessian for faster convergence. We used the initial Hessian matrix contemplated in the Schlegel 2 model [22]. CRYSTAL17 set the convergence criteria around the root mean square of both the gradient and the displacement by default. It required six optimization cycles for the tetragonal structure and four for the cubic one.

3. RESULTS AND DISCUSSION

3.1. Electronic properties

This section shows each of the charge density-dependent electronic characteristics and associated physical parameters that describe the electronic behavior of the hydrides under study in both the direct and reciprocal lattices. A MAPNET point grid allowed us to have access to 2D and 3D representations of the charge density and electrostatic potential, as well as to representations of their derivatives. The energy as a function of given directions of the reciprocal space framed in highly symmetrical points of the first Brillouin zone was also presented, as well as the density of states as a function of energy and the electronic behavior within the material deduced from the orbital overlap and Hamiltonian population.

pISSN: 0255-6952 | eISSN: 2244-7113
Rev. LatinAm. Metal. Mat. 2023; **43** (2): 95-115

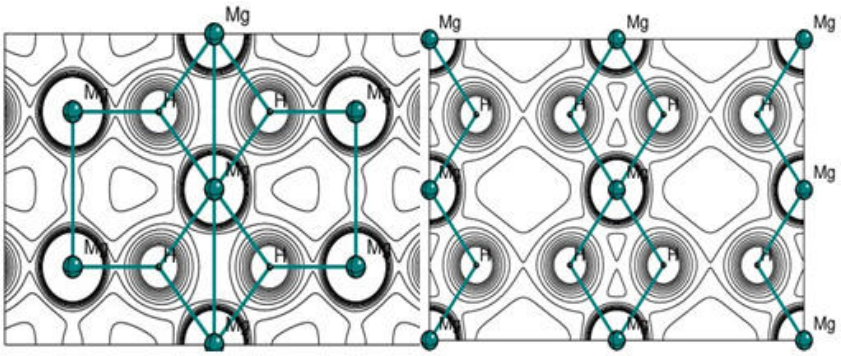

Figure 1. *Contour lines of the electron charge density projected on the (-1,1,0) plane. a. α-MgH_2 b. β-MgH_2*

3.1. 1.- Electron charge density

We calculated the electron charge density on the plane associated with points (0 01), (0 0 0 0), and (1 10) of a 61800-point rectangular grid. Figure 1 presents the charge density contour lines for each hydride, and Figure 2 depicts charge density maps. The difference between the total charge density and that generated by the orbital overlap and electrostatic potential maps highlights the denser charge distribution around the Mg atoms, whose atomic basin, on account of its electron configuration, is larger than that of H.

In α-MgH_2 (Fig. 2b), the largest detected charge density difference occurred around the edges containing the atomic centers. However, this difference, which indicates that the superposition of atomic orbitals does not cover the total density in these spaces, is not greater than 0.02 e $bohr^{-3}$. In the β-hydride (Fig. 2e), the difference was detected in the empty atomic regions, with values 10 times lower than those reported in the α-hydride. At this level, a priori calculations using different basis sets revealed detectable variations in the electronic charge density maps. Figures 2.c and 2.f display the electrostatic potential maps for each hydride. The curves illustrate the high potential around each atomic nucleus. This high potential is shown in white for Mg atoms due to the absence of electrons and in red for H atoms. As we move away from the atomic nuclei, the potential gradually decreases towards the interstitial region. In fact, negative values of lower potential intensity (not shown in the figure) have been detected in this region.

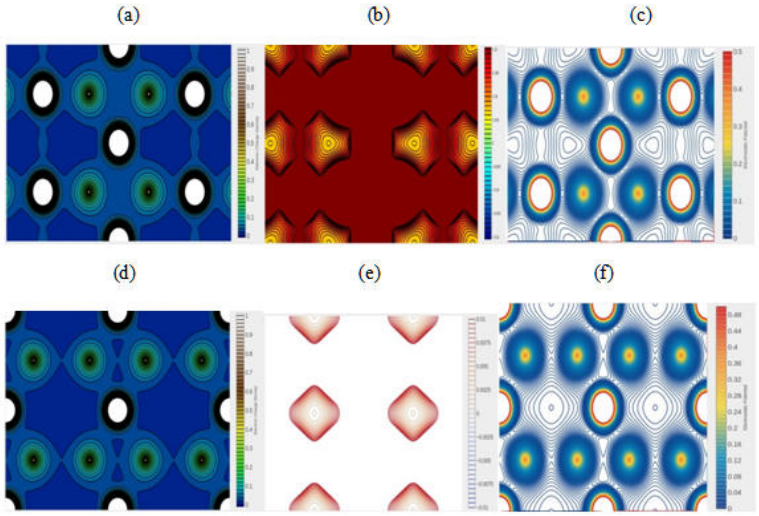

Figure 2. Maps of the electron charge density (a, d). Difference between the total charge density and that obtained by superposition of the atomic orbitals (b, e). Maps of the electrostatic potential (c, f). a, b, c: α-MgH_2. d, e, f: β-MgH_2

pISSN: 0255-6952 | eISSN: 2244-7113
Rev. LatinAm. Metal. Mat. 2023; **43** (2): 95-115

3.1.2.- Electron bands and density of states

Figure 3 shows the electronic band structure and density of states for each hydride.

The electron band structure was calculated on symmetry directions defined between high symmetry points of the first Brillouin zone. In the tetragonal α-MgH_2 (Fig.3a), bands 11 through 36 were checked in the energy ranges, ΔE, shown in Table 2. The selected path in the first Brillouin zone was ΓXMΓZRAZXΓ, reporting a Fermi energy of -0.16421 a.u. The alpha-hydride showed an insulating character with indirect energy band gaps of 3.9651 eV (0.146 a.u.) Although the literature reports values of 3.73 eV (0.137 a.u.) [10] and 3.8 eV (0.1396 a.u.) [19], 3.7327 eV (0.137 a.u) (ICSD), 3.71 eV (0.136 a.u) (mp) for this gap, the value measured in situ by both ellipsometry and spectrophotometry was 5.6 eV (0.206 a.u.) [23]. Using the GW-projector-augmented-wave approach, Araujo et al. [24] found an indirect band gap of 5.58 eV (0.205 a.u.) and a direct band gap of 6.52 eV (0.24 a.u.), showing a better agreement with the experimental values.

Bands 7 through 22 along the ΓXLWKΓ path were also checked in the FCC β-MgH_2 (Fig. 3b). This hydride showed a conducting character in agreement with the results reported in References [10,19], with a clear intersection of the Fermi level with the energy bands at the Γ and K points of the first Brillouin zone, and with a Fermi energy of

-0.03128 a.u. In contrast to this behavior, the β-MgH_2 hydride in Ref. [24] showed an insulating character with direct and indirect gap bands of 4.74 eV (0.174 a.u.) and 3.90 eV (0.143 a.u.), respectively, and a bandwidth of 0.173 a.u. at Γ, whereas in this work, the bandwidth at Γ was 0.338 a.u., a difference mainly related to the calculation scheme used. In general, all hydrides studied in Ref. [24] show an important energy gap, which in principle gives them the character of insulators, but their lack of explicit indication of the Fermi level prevents us from determining if there is an overlap of this level with the valence bands. Note that if these bands were referenced to the Fermi level, as in our case, a possible crossover with this level might occur.

The Fermi levels obtained in this work were lower than those reported in Ref. [10], which points out values of 0.022232 a.u. and 0.131425 a.u. for the respective hydrides, indicating the dependence of this scheme on the basis sets selected.

Although both hydrides showed fewer valence bands than conduction bands in Figure 3 and the energy range given in Table 2, a set of degenerate and highly localized valence bands of p-orbitals of Mg has been detected for energy values of -1.5 a.u. for α-MgH_2 and -1.6 a.u. for β-MgH_2.

The density of states, DOS, was calculated on a fine mesh: one of 405 k-points for the α-MgH_2 (Fig. 3a) and one of 145 k-points for the β-hydride (Fig. 3b), in three projections, two corresponding to the s and p orbitals of Mg and one to the s of Hydrogen.

Both hydrides show a significant contribution from the s-H and p-Mg orbitals to the valence bands below the Fermi level, with a minor contribution from the s-Mg orbitals. The conduction bands consist mainly of Mg orbitals. DOS also shows a significant localized contribution from the p-Mg orbitals, around -1.5 a.u.

Table 2, showcasing aspects of interests related to this evaluation, highlights the details of these projections and the effect of basis set selection on the projection of both partial integrated (PID) and total integrated (TID) densities in the respective energy intervals by ΔE projection. We noticed the dominant character of the p orbitals of Mg in these projections, the contribution of s-PID of H being larger than that of s-PID of Mg in both hydrides.

3.2. Overlapping and Hamiltonian population of crystalline orbitals (COOP and COHP)

Although the density of states refers to the contribution of an orbital or set of atomic orbitals to the electronic structure of the material, as shown in Figure 3, it does not provide information about the interaction between orbitals. Based on the same mathematical formulation for the density of states, we partitioned the electron density by projecting orbitals onto those of other atoms, thus accessing overlapping orbitals when it was the overlap matrix the one involved (COOP); or the Hamiltonian orbital population when the Hamiltonian matrix was involved (COPH), both integrated over the first Brillouin zone. Both COOP and COHP are basis-

pISSN: 0255-6952 | eISSN: 2244-7113
Rev. LatinAm. Metal. Mat. 2023; **43** (2): 95-115

dependent.

Table 2. Projection of the atomic orbitals on the DOS for α and β hydrides

Hydride	K	AO	N	PID	TID/Bands	ΔE (a.u.)
α-MgH_2	405	s Mg	1-5	1.88236	52/11-36	-0.41658
		p Mg	6- 14	5.86356		
		s H	39 - 41	3.04660		1.07610
β-MgH_2	145	s Mg	1-5	1.76149	32/7-22	-0.26271
		p Mg	6-14	6.35787		
		s H	20-22	2.65387		1.85785

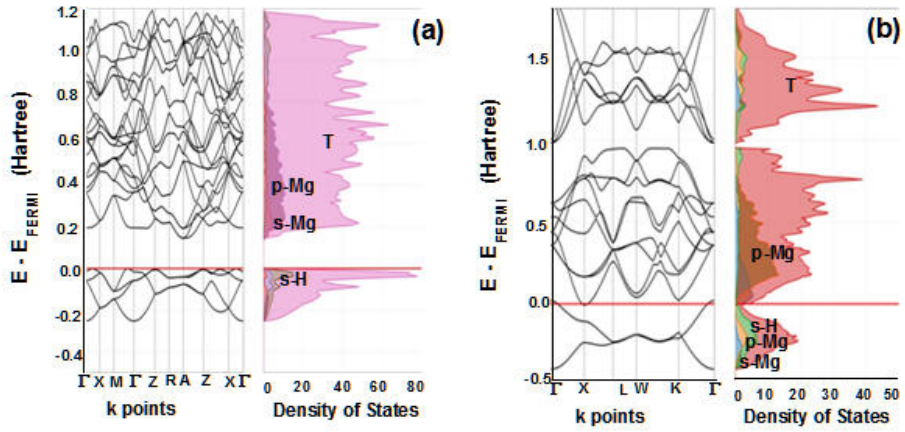

Figure 3. Band diagram and density of states for the hydrides studied. (a) α-MgH2. (b). β-MgH2The partial contribution of the s and p orbitals of Mg and that of s of H are included in the DOS plot. T represents the total density of states.

The area under the curve of such partitions as a function of energy is related to the bonding or antibonding character of the group of orbitals considered, the integrated COOP being associated with bond order; and the integrated COHP, with bond strength [25-27].

Considering that bond orbitals are more stable than antibond orbitals, their energy being thus lower; and that the Hamiltonian matrix has an opposite sign to the overlap matrix [28], a bond state can be associated with a negative Hamiltonian population of crystallographic orbitals (-COHP) or with a positive overlapping population of crystallographic orbitals (COOP), while the antibond states would be associated with positive COHP and negative COOP. However, this consideration is not absolute since COHP depends on the energy scale reference or zero energy.

Our COOP and COHP calculations, performed on a k-point grid like that used when calculating DOS, are shown in Figure 4. Unlike the DOS calculations, all the orbitals defined in the respective Mg basis sets, located at the origin of our unit cell and projected on all the hydrogen orbitals at position (2.585, 2.585, 0.) for the α-hydride; and (2.252, -2.252, -2.252) for the β-hydride (both in Bohr), participated. COOP is represented in that figure by the black area, while COHP is represented by the green one, the COOP units being the same as those of DOS (states/Hartree/cell) and COPH (states/cell).

Figure 4 shows the presence of bonding, antibonding and nonbonding states over the entire energy range considered. Figures 4.a and 4.b demonstrate the prevalence of anti-bonding states for COOP (negative) and COHP (positive) above the Fermi level when projecting H orbitals onto Mg orbitals. In Figure 4.c, corresponding to the projection of the s orbitals of hydrogen onto the p

pISSN: 0255-6952 | eISSN: 2244-7113
Rev. LatinAm. Metal. Mat. 2023; **43** (2): 95-115

orbitals of Mg, a similar behavior is observed, but not in the s-s projection of hydrogen shown in Figure 4.d, where a competition between bonding and antibonding orbitals is observed over the whole energy range shown. In contrast, the bonding states for both COOP (positive) and COHP (negative) are shown in the region of higher electron occupancy, just below the Fermi level in both β-MgH_2 and α-MgH_2.

Table 3 shows the integrated COOP and COHP values for the occupation down to the Fermi level, in agreement with Hugbanks et al [26]. The table presents the interaction between Mg and H orbitals in α and β hydrides. So are the values for the Mg-Mg interaction of the α-MgH_2 at positions (0, 0, 0) and (4.246, 4.246, 2.840) a.u. and for the H-H interaction in the β-MgH_2 at positions (2.252, -2,252, -2.252) and (-2.252, -2,252, -2.252) a.u. The negative sign in the antibonding population only indicates the character of the interaction between the selected pair of atoms.

The bond character and bond strength can be relatively established from Figure 4 and Table 3. The integrated COOP includes all bonding and antibonding states of the Mg-H, Mg-Mg, and H-H interactions of both hydrides over the entire energy range studied and shows a higher magnitude for the cubic structure than for the tetragonal one, indicating a higher bonding order of β-MgH_2 relative to that of α-MgH_2. This behavior is consistent with the integrated COHP, which also shows a higher binding strength in this energy range for the β-hydride.

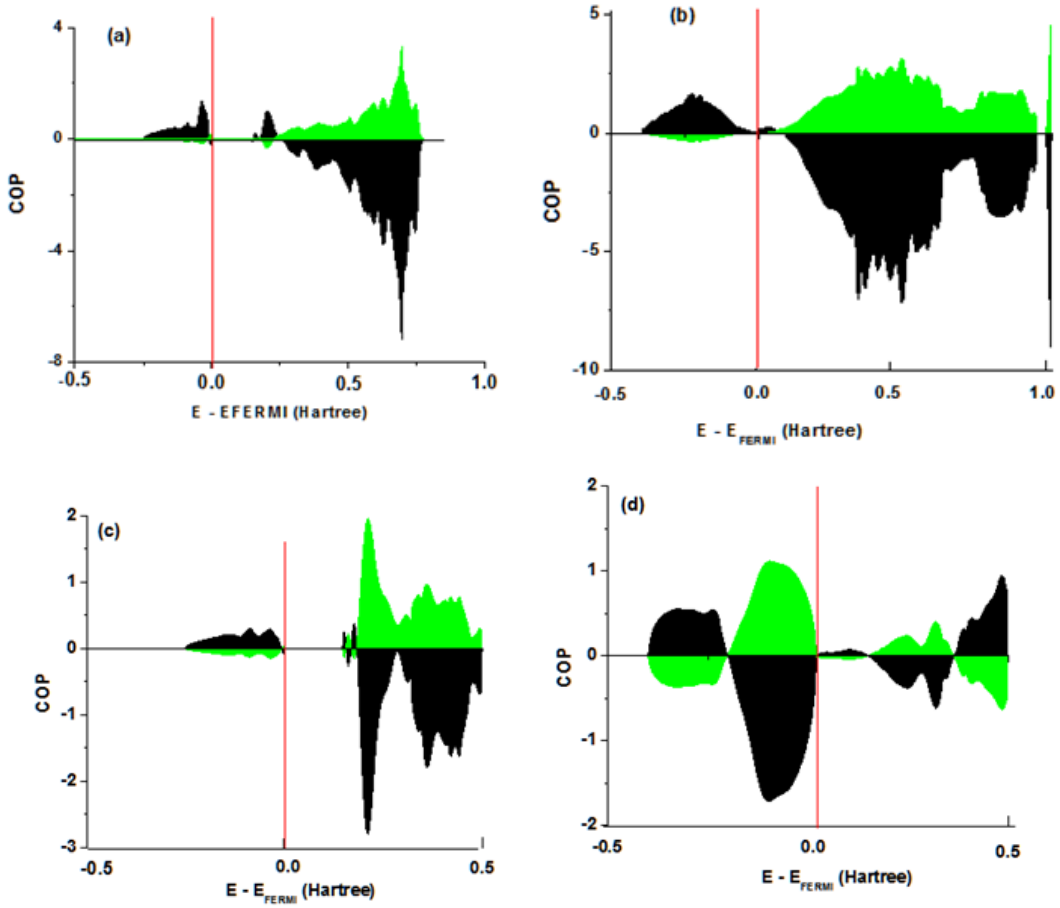

Figure 4. Crystalline Orbital Population (COP) as a function of energy. (a) For H orbitals projected onto Mg orbitals in the α-hydride. (b) H orbitals projected onto Mg orbitals in the β-hydride. (c) Mg orbitals projected onto orbitals of a neighboring Mg atom in α-MgH_2. (d) H orbitals projected onto orbitals of a neighboring H atom in β-MgH_2. In black: COOP. In green: COHP.

pISSN: 0255-6952 | eISSN: 2244-7113
Rev. LatinAm. Metal. Mat. 2023; **43** (2): 95-115

The COOP and COHP behavior of the occupied states [29] defines both the binding order and the binding strength of the considered hydride. The bond population and binding energy in Table 3 show that for the bound states, the bond order is higher in the β-hydride than in the α-hydride, and the binding energy is higher in the β-hydride than in its α-hydride counterpart, a result consistent with the thermodynamic fact that α-hydrides are more stable than β-hydrides [30,10]. The dominant weight over COOP/COHP of the s-H orbital projection over the p-Mg orbitals is also shown in Table 3.

The analysis of the Mg-Mg interaction in α-hydride reveals an integrated orbital population down to the Fermi level, with bonding states prevailing over anti-bonding states. In contrast, the H-H interaction in β-hydride is dominated by anti-bonding states. It is important to note that this calculation includes the p-orbitals of Mg detected around -1.5 Hartree. In summary, the table shows the occurrence of bonding states between Mg-H and Mg-Mg orbitals, as well as anti-bonding states between H-H orbitals, when the bonding population is considered over all the occupied states.

Table 3. Integrated values of COOP and COHP for the two Mg-H interactions in α-MgH_2 and β-MgH_2, and for Mg-Mg interactions in α-MgH_2 and H-H in β-MgH_2, for the occupation down to the Fermi level. The integrated COOP values are expressed in units of State/cell, and the integrated COHP values are expressed in State.Hartree/cell units.

	Integrated COOP	Bonding population	Antibonding Population	Integrated COHP	Bonding energy	Antibonding energy
α-MgH_2 Mg-H	0.10772	0.108950	-0.00123	-0.01586	-0.01753	0.0187
β-MgH_2 Mg-H	0.31896	0.31896	-0.00	-0.06918	-0.06918	0.00
α-MgH_2 Mg-Mg	0.04357	0.0441	-0.00053	-0.02093	-0.02093	0.0
β-MgH_2 H-H	-0.15512	0.09018	-0.2453	0.10244	-0.09016	0.1926
α-MgH_2 sH-pMg	0.05688	0.057160	-0.0028	0.01582	-0.01512	0.03094
β-MgH_2 sH-pMg	0.16219	0.16219	0.0	-0.0370	-0.0370	0.0

3.3. Topology

By following the guidelines expressed in our previous work [10], valuable information can be obtained from the study of maxima and minima of characteristic functions of the interaction between atoms in a solid. However, much information associated with each of the scalar fields defining the Hamiltonian was not included in that work, and we propound that not only the topology of the charge density but also the topologies of its Laplacian and that of the potential energy density and kinetic energy are important elements in a global definition of bonds in materials. The charge density topology did not allow us to visualize the atomic layer structure, secured by the charge density Laplacian topology evincing the electron pairs of the Lewis model [29].

The mathematical behavior of the scalar function charge density, an aspect on which Bader based his theory of atoms and molecules [31], involved a study of the continuity of this function in an atomic region perfectly delimited by the gradient of the charge density ($\nabla\rho.\mathbf{n}=0$) and a vector normal to the gradient lines, which configured a physical space or atomic basin for each of the atoms. The maxima and minima of the charge density, where the gradient cancels out, defined the critical points of this function, while its behavior, characterized by the curvatures at these points, was given by the second derivative of the charge density, specifically through the Hessian matrix. To define the CP (r, s), we used the number of nonzero eigenvalues (rank) and their sign (signature) in this matrix. The 3-D crystals are rank 3 and the curvatures can be all negatives (-3) or nucleus CP (3, -3), two negative

pISSN: 0255-6952 | eISSN: 2244-7113
Rev. LatinAm. Metal. Mat. 2023; **43** (2): 95-115

curvatures and one negative (-1) or bond CP (3, -1), two positive curvatures and one negative (+1) or ring CP (3, 1), and three positive curvatures (+3) or cage CP (3, 3) [32,11]. These four elements configured the chemical structure of the crystal associated with the observable original provided by the charge density.

Other scalar functions involved in the Hamiltonian defining the electronic behavior of atoms, such as the negative Laplacian of the charge density ($-L(r)=\nabla^2\rho$) [33, 34], the potential energy density K(r), and the kinetic energy density G(r) [35], presented their own topological configuration; and their study and consideration allowed for the differentiation of details associated with atomic bonds not detectable with the use of the charge density topology alone [36, 11]. The topology of these scalar functions was evaluated within the scheme provided by CRYSTAL17 and related TOPOND programs [37-40], which provided the critical points of the scalar functions under consideration and determined the atomic basins and their properties, all supported by a friendly graphical representation scheme.

3.3.1.Topological Analysis of the Electron Charge Density

Crystal17 uses different strategies to determine the CPs of the charge density of a molecule or a solid, but it does not do this on the whole periodic structure; instead, starting from a point in the crystal, it constructs an atomic subset or cluster representative of the interactions of that crystal, reducing the mathematical and computational complexity of analyzing scalar functions on the whole crystal and exploiting the local features around selected atoms or groups of atoms, thus revealing details about atomic bonding patterns and their coordination, as well as localized aspects of the electron charge density around these bonds.

The atomic clusters are approximations to the whole crystal, which, through their well-defined dimensions and contours, reduce the drawbacks imposed by the translational symmetry of the crystal. The results presented below follow the scheme defined by IAUTO = -1, where the search for CPs is automatically and separately performed according to the sequence (3,-3), (3,-1), (3,+1), and (3,+3) in a region defined as the union of spaces of molecular clusters centered on each of the nonequivalent atoms of the unit cell [36]. In our case, a cluster of 46 atoms around nonequivalent Mg and another of 23 atoms around nonequivalent H were used for α-MgH_2, while for the β-MgH_2, a cluster of 190 atoms around the Mg and 124 atoms around the nonequivalent H, were fixed.

CPs were automatically located by the algorithm suggested by Popelier [39] and adapted to TOPOND by Gatti *et al*. [3]. The CPs identified in the charge density of the hydrides studied correspond to two nucleus CP, three CP bonds, and three CP rings for the tetragonal structure; and two nucleus CP, two CP bonds, one CP ring, and one CP cage for the cubic one. The difference with the number of CPs reported in Ref. [10] comes from the calculation strategy, since only the CP bonds around the nonequivalent atom clusters selected were identified in this work. Although the topological study was performed on clusters as a strategy to evaluate the local maxima and minima of the scalar functions involved, at no time was the particular electron density of each cluster re-evaluated, but the electron density of our original system was still used, as confirmed in Section 4.3c. CRYSTAl17 provides a detailed output of each cluster around the selected equivalent atom and all neighboring layers up to a given limit.

The bond characteristics were reflected on the bond CPs, detailed in Table 4, which features the position of the bond CP in Å, the atoms involved in the bond, its location with respect to the reference cell, and its distance to the respective CP. Two Mg-H bonds and one H-H bond were identified for α-MgH_2; and one Mg-H bond and one H-H bond were identified for β-MgH_2. The reported values were in agreement with those of Luiggi [10], who reported bond lengths of 1.853 Å - 1.835 Å and 1.818 Å - 1.837 Å for the Mg-H, and of 2.3492 Å - 2.3492 Å for the H-H, in the α-MgH_2; and 1.8998 Å - 2.0020 Å for the Mg-H bond and 2.2527 Å - 2.2527 Å for the H-H bond in the β-MgH_2, the reported values being concordant in each case.

pISSN: 0255-6952 | eISSN: 2244-7113
Rev. LatinAm. Metal. Mat. 2023; **43** (2): 95-115

Table 4. CP bonding of ρ(r) of MgH_2

Hyd	X(Å)	Y(Å)	Z(Å)	ρ	$\nabla^2\rho$	Bond	Position	Length
α-MgH_2	0.674	0.674	0.000	0.030	0.115	H-3	0, 0, 0	1.796
						Mg-1	0, 0, 0	1.801
	0.417	-0.417	-0.756	0.030	0.110	Mg-1	0, 0, 0	1.811
						H-6	0, 0, -1	1.848
	-2.215	-2.215	0.000	0.021	0.015	H-4	0, 0, 0	2.322
						H-3	-1, -1, 0	2.322
β-MgH_2	0.571	-0.571	-0.571	0.024	0.083	Mg-1	0, 0, 0	1.870
						H-2	0, 0, 0	1.989
	1.179	0.000	-1.179	0.020	0.010	H-2	0, 0, 0	2.228
						H-3	0, 0, 1	2.228

3.3.2. Topological Analysis of the Electron Charge Density Laplacian

Securing critical points of $\nabla^2\rho$, corresponding to $[\nabla(\nabla]^2\rho) = 0$, is the main goal of charge density Laplacian topology studies. The sign of the Laplacian of the electron charge density at the point under evaluation expressed the behavior of the charge density at that point. $\nabla^2\rho > 0$ implied a low charge density and charge depletion in the region surrounding that point. $\nabla^2\rho < 0$ implied a locally concentrated charge density, $\nabla^2\rho$ thus playing an important role in the chemical bond classification. The presence of the charge density Laplacian in functions such as ELF, kinetic energy density, total electron energy density [41], $h(r) = g(r) + v(r)$, and the virial theorem [27], $2g(r) + v(r) = \frac{1}{4}\nabla^2(\rho(r))$, provided extra information on charge depletion and concentration around the critical points, preferentially the CP nucleus and CP bond, which allowed for a more complete assessment of the chemical bond than that provided by the electron charge density alone. An extensive discussion of the use of these functions in the interpretation of chemical bonding is presented by Gatti [11].

CP determination of the charge density Laplacian for both hydrides was performed on two clusters of atoms, one of 32 atoms around nonequivalent Mg and another of 28 atoms around nonequivalent H for the tetragonal structure; while for the cubic hydride, the respective clusters comprised 50 and 48 atoms, respectively. The search for the CPs was done by means of the eigenvector following (EF) numerical procedure.

Tables 5 and 6 detail the characteristics of the CPs covered, indicating, for each nonequivalent atom considered, the Wyckoff positions in the cell under consideration, the multiplicity, CP type, its distance to the reference atomic nucleus, value of -L(r), ρ(r), and the eigenvalues of the Hessian matrix that define CP type, as well as the sign of the contributions of g(r), v(r), and h(r) to the respective bond critical point, which defines the character of such a bond.

Many CPs were detected in the preconfigured clusters because of the higher number of maxima and minima located in the gradient of the Laplacian. For α-MgH_2, 45 CPs were recovered around nonequivalent Mg: 28 (3, -1) bonding CPs (Bcp) fell within the Mg VSCC and 17 (3, -3) charge concentration maxima CPs (Ncp). Six of the latter were positioned on H atoms at Wyckoff positions f and j; and the other 11, on hydrogens, far away from the respective CPs. Around the nonequivalent H, 12 CPs were detected, all of them having already been detected in the previous search, and of course, far away from the H VSCC.

For β-MgH_2, 98 CPs were recovered around nonequivalent Mg, 72 of them falling within Mg VSCC (16 Rcp at position j, 16 Bcp at k, and 40 Bcp at I) and 25 around nonequivalent H (12 Bcp

pISSN: 0255-6952 | eISSN: 2244-7113
Rev. LatinAm. Metal. Mat. 2023; **43** (2): 95-115

detected in the previous search at positions k and j, away from H VSCC, and 13 Ncp already covered in the search around nonequivalent Mg). For both hydrides, every Bcp showed an ionic character (CSI: Close Shell - Ionic) according to the classification of atomic interactions proposed in Ref. [11].

Table 5 reflects a value of $-\nabla^2(\rho(r) > 0$ for the α-MgH_2 at the Ncp belonging to Mg at Wyckoff positions f and j with a charge density of 0.381 a.u., this value remaining negative (*i.e.*, positive L(r)) for other critical points even at the Ncp corresponding to H located at Wyckoff positions i and e with a charge density up to 10 times lower. In Table 6, for the β-MgH_2, the condition of $-\nabla^2(\rho(r) > 0$ was satisfied for the Ncp of Mg at position f with a charge density of 0.376 a.u., while those corresponding to H were located at positions e, h, and j, with $-\nabla^2(\rho(r) < 0$ and with a much lower charge density. This analysis confirmed the charge concentration around the Mg atoms and a depletion around the other CPs. When a charge depletion was detected, the H atoms were closer to the respective CPs.

Table 5. CP characteristics of the Charge density Laplacian for the α-MgH_2, all expressed in a.u.

WP	Mult	Type	Rx (au)	-LAP	RHO	λ1	λ2	λ3	g/ -v/- h / I
CP search for nonequivalent atom Mg. Sphere radius: 2.5499 a.u.									
K	**8**	**(3,-1)**	**2.136**	**-0.020**	**0.016**	**-0.036**	**-0.007**	**0.008**	**+/+/+/CSI**
K	**8**	**(3,-1)**	**2.555**	**-0.015**	**0.008**	**-0.014**	**-0.003**	**0.004**	**+/+/+/CSI**
i	**4**	**(3,-3)**	**3.027**	**-0.013**	**0.004**	**-0.010**	**-0.003**	**-0.001**	
i	**4**	**(3,-1)**	**1.546**	**-0.021**	**0.031**	**-0.115**	**-0.002**	**0.101**	**+/+/+/CSI**
e	**2**	**(3,-3)**	**2.323**	**-0.015**	**0.021**	**-0.025**	**-0.011**	**-0.006**	
f	**2**	**(3,-3)**	**0.000**	**23.115**	**0.381**	**-1000**	**-1000**	**-1000**	
j	**5**	**(3,-3)**	**2.171**	**-0.014**	**0.014**	**-0.046**	**-0.016**	**-0.001**	
j	**4**	**(3,-1)**	**1.556**	**-0.021**	**0.034**	**-0.028**	**-0.013**	**0.111**	**+/+/+/CSI**
j	**4**	**(3,-3)**	**0.000**	**23.115**	**0.381**	**-1000**	**-1000**	**-1000**	
j	**4**	**(3,-1)**	**1.549**	**-0.019**	**0.032**	**-0.094**	**-0.006**	**0.098**	**+/+/+/CSI**
CP search for nonequivalent atom H. Sphere radius: 0.7181 a.u.									
j	**2**	**(3,-1)**	**1.549**	**-0.019**	**0.032**	**-0.094**	**-0.006**	**0.098**	**+/+/+/CSI**
j	**2**	**(3,-3)**	**2.171**	**-0.014**	**0.014**	**-0.046**	**-0.016**	**-0.001**	
j	**2**	**(3,-1)**	**1.556**	**-0.021**	**0.034**	**-0.028**	**-0.013**	**0.111**	**+/+/+/CSI**
i	**2**	**(3,-1)**	**1.546**	**-0.021**	**0.031**	**-0.115**	**-0.002**	**0.101**	**+/+/+/CSI**
i	**2**	**(3,-3)**	**3.027**	**-0.013**	**0.004**	**-0.010**	**-0.003**	**-0.001**	
f	**1**	**(3,-3)**	**0.000**	**23.115**	**0.381**	**-1000**	**-1000**	**-1000**	
f	**1**	**(3,-3)**	**2.323**	**-0.015**	**0.021**	**-0.025**	**-0.011**	**-0.006**	

pISSN: 0255-6952 | eISSN: 2244-7113
Rev. LatinAm. Metal. Mat. 2023; **43** (2): 95-115

Table 6. CP characteristics of the Charge density Laplacian for the β-MgH_2

WP	Mult	Type	Rx (au)	-LAP	RHO	λ1	λ2	λ3	g/ -v/- h / I
CP search for nonequivalent atom Mg. Sphere radius: 2.5499 a.u.									
j	**16**	**(3,+1)**	**2.569**	**-0.019**	**0.012**	**-0.019**	**0.000**	**0.007**	**+/+/+/CSI**
i	**40**	**(3,-1)**	**2.483**	**-0.019**	**0.012**	**-0.021**	**0.000**	**0.006**	**+/+/+/CSI**
e	**6**	**(3,-3)**	**3.859**	**-0.012**	**0.002**	**-0.009**	**-0.009**	**-0.009**	
h	**12**	**(3,-3)**	**2.293**	**-0.018**	**0.019**	**-0.039**	**-0.017**	**-0.005**	
k	**16**	**(3,-1)**	**1.603**	**-0.022**	**0.030**	**-0.016**	**-0.003**	**0.033**	**+/+/+/CSI**
f	**8**	**(3,-3)**	**0.000**	**22.741**	**0.376**	**-1000**	**-1000**	**-1000**	
CP search for nonequivalent atom H. Sphere radius: 0.7181 a.u.									
k	**6**	**(3,-1)**	**1.603**	**-0.022**	**0.030**	**-0.106**	**-0.003**	**0.033**	**+/+/+/CSI**
i	**6**	**(3,-1)**	**1.603**	**-0.022**	**0.030**	**-0.106**	**-0.003**	**0.033**	**+/+/+/CSI**
j	**2**	**(3,-3)**	**2.293**	**-0.018**	**0.019**	**-0.039**	**-0.017**	**-0.005**	
i	**6**	**(3,-3)**	**2.293**	**-0.018**	**0.019**	**-0.039**	**-0.017**	**-0.005**	
f	**1**	**(3,-3)**	**0.000**	**22.741**	**0.376**	**-1000**	**-1000**	**-1000**	
h	**4**	**(3,-3)**	**2.293**	**-0.018**	**0.019**	**-0.039**	**-0.017**	**-0.005**	

The numerical details of Tables 5 and 6 are visualized in Fig. 5, for the α-MgH_2, and Fig. 6, for the β-MgH_2, where the electron density and the trajectories defined by the charge density gradient $\nabla\rho = 0$, as well as the projected Laplacians and the respective trajectories, are shown. The projection planes in both cases correspond to those defined in Fig. 1.a and 1.b, respectively.

In both hydrides, the projections of the electron charge density correspond to density peaks in the atomic positions of the Mg and H atoms, whose magnitude, owing to their electronic configuration, decreased as we moved away from these positions. The basins associated with Mg are of a greater intensity than those of H (part a of both figures). The Ncp are highlighted in the center of the Mg atoms, whose ρ value is maximum, while the Bcp are located in the path joining the Mg and H atoms.

As for the Laplacian, it highlights the positive value of this scalar function at the atomic sites of Mg, and the negative around the atomic sites of H. Note that in both figures, the trajectories plotted in Figs. 5 and 6 correspond to the gradient of the electron charge density and the Laplacian gradient of the electron charge density.

Crystal17 also deployed a series of programs aimed at evaluating and visualizing different scalar functions such as the electronic localized function (ELF), the energy potential density (KKIN), and the virial density. Figure 7, like Figure 1 for α and β hydrides, shows these results on crystallographic plane (-1,1,0). For ELF, the intensity sequence plotted from highest to lowest is white, violet, and green (starting from the H atoms), preconfiguring an ELF profile with a maximum at the center of H, its gradual decrease down to a minimum ELF (green) at the boundary with other atoms, from which it increases up to the central position of another neighboring atom. The white regions between Mg-Mg, H-H, and Mg-H are a consequence of the step selected for the calculation, but an ELF map shows such regions in green, corresponding to a minimum ELF. The electron

pISSN: 0255-6952 | eISSN: 2244-7113
Rev. LatinAm. Metal. Mat. 2023; **43** (2): 95-115

localization function indicated the probability of finding an isolated or bonded electron pair in a region of the crystal, showing high localization for the highest ELF values, found around the H atoms and manifested as white basins in the figure. As for the Mg atoms, a maximum of ELF was detected at its center with a layered distribution around it, where ELF fluctuated between maximum and minimum values, a normal behavior in functions where the scalar Laplacian is involved.

The potential energy density reading indicates a positive value in both atomic nuclei (white), the value in Mg being much higher than that in H. The violet ring denotes a positive density that degraded to a null value and then became negative (depicted in green) up to the contour with the H atom. The potential energy density around H always remained positive and decreased from the center to its outer contour, its magnitude being lower in H than in Mg. The atomic inter-region maintained a null value of KKIN.

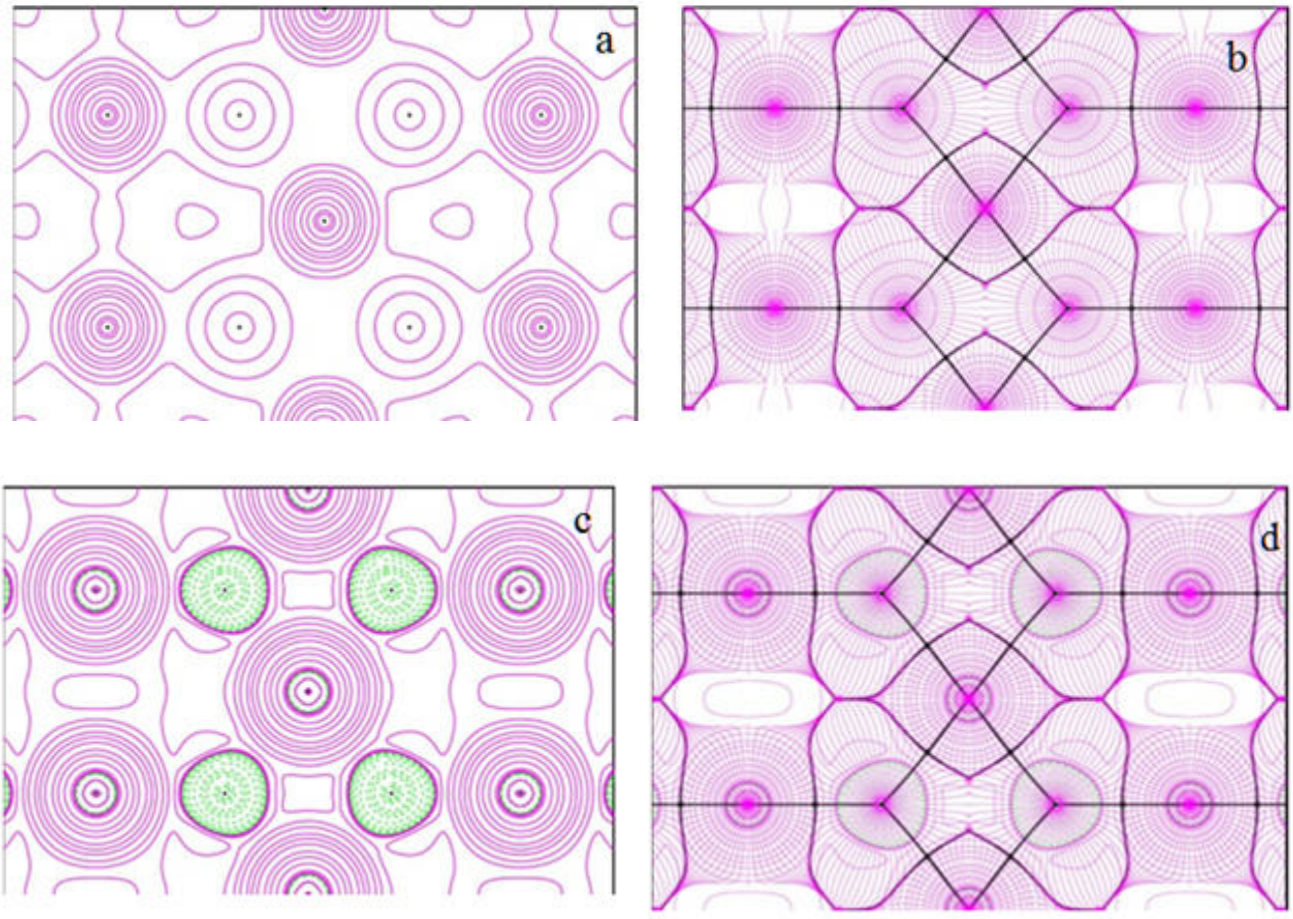

Figure 5. *Projected electron density and projected Laplacian of α-MgH_2 a. Electron density (ρ).* b. Gradient trajectories ($\nabla\rho$) mapped on a total electron density plot considering a crystal graph defined by Mg atoms in the (0,0,-1) and (0,0,0) cells; H atoms in the (0,0,-1) cell plotted (contour levels at 0.02 e A˚-3) . c. Laplacian of the electron density ($\nabla^2\rho$). d. Laplacian Gradient trajectories $\nabla(\nabla^2\rho)$ mapped on the Laplacian of the charge density. Green lines indicate negative contour levels. Bond paths are indicated in heavy black lines and critical points (identified in Table 5) are denoted by small black circles. Atom positions of Mg and H are as in Fig. 1a.

pISSN: 0255-6952 | eISSN: 2244-7113
Rev. LatinAm. Metal. Mat. 2023; **43** (2): 95-115

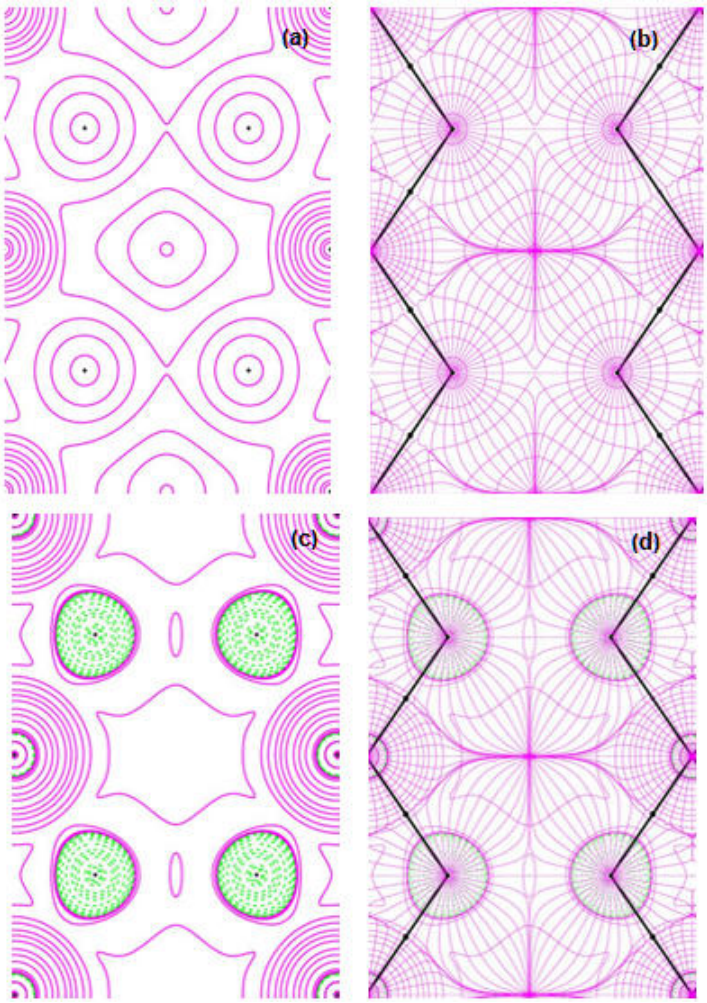

Figure 6. *Projected electron density and projected Laplacian of β-MgH_2 a. Electron density (ρ). b. Gradient trajectories ($\nabla\rho$) mapped on a total electron density plot considering a crystal graph defined by H atoms in the (0,1,0) and (0,0,0) cells; Mg in the (-1,0,0) cell (contour levels at 0.02 e A°-3) c. Laplacian of the electron density($\nabla^2\rho$). d. Laplacian Gradient trajectories $\nabla(\nabla 2\rho)$ mapped on the Laplacian of the charge density. Green lines indicate negative contour levels. Bond paths are indicated in heavy black lines and critical points (identified on Table 6) are denoted by small black circles. Atom positions of Mg and H are as in Fig. 1b*

As for the virial density, it varied from a negative minimum in the mid region between atoms, increasing negatively up to the atomic center, the value reached at the center of the Mg atom having a higher negative magnitude than that reached in the H atom.

pISSN: 0255-6952 | eISSN: 2244-7113
Rev. LatinAm. Metal. Mat. 2023; **43** (2): 95-115

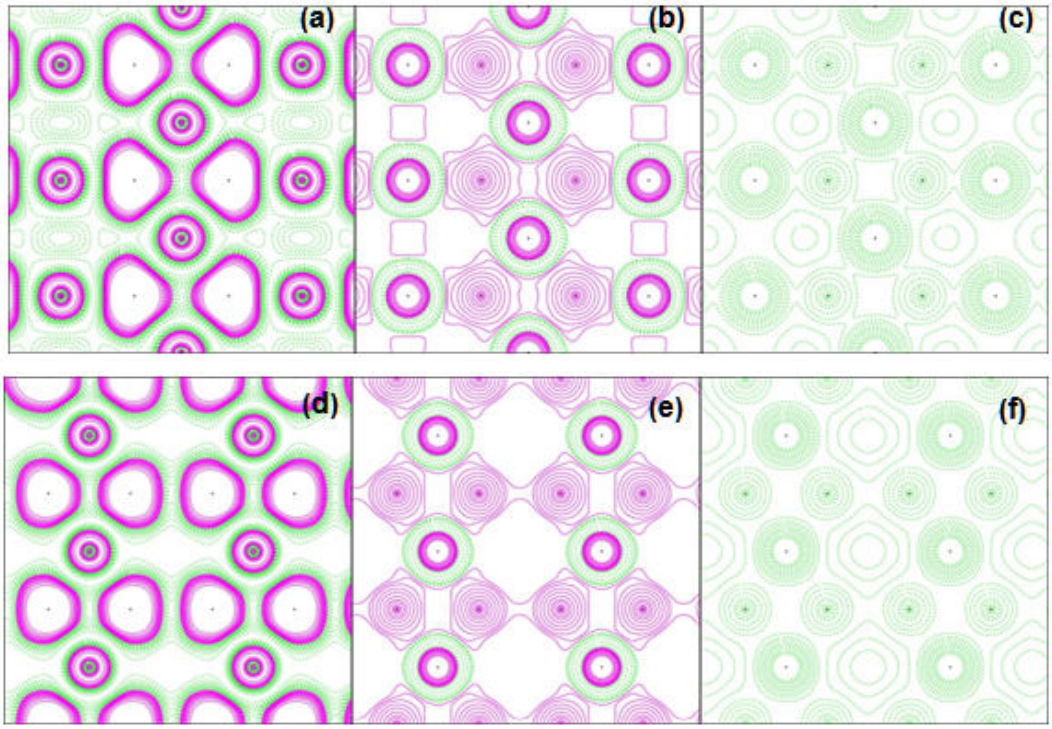

Figure 7 *Topologies of scalar function of α and β hydrides. a, b, c: For α hydrides. d, e, f: for β hydrides. a, d: Electron localized function. b, e: Energy potential density (KKIN). c, f: Virial density.*

3.3.3. Properties of atomic basins

Atomic basins, Ω, are regions bounded by surfaces $S(\Omega,r_S)$ whose points r_S satisfy the zero flux condition, ZFS, $\nabla\rho(r_S).n(r) = 0$, where $n(r)$ is a vector normal to the surface. The average atomic properties were evaluated by integrating the distribution density of that property over its respective atomic basin. Our calculations were performed on the basins of all nonequivalent atoms, adopting pre-established standard parameters and considering the absence of non-nuclear attractors.

The properties were calculated on clusters of 46 atoms around nonequivalent Mg and 23 atoms around nonequivalent H for the tetragonal structure of α-MgH_2, and clusters of 214 and 124 atoms for the cubic structure of β-MgH_2.

The populations and atomic energies evaluated in the Mg and H basins for both hydrides are shown in Table 7. N is the average basin electron population, Q is the net charge, L is the atomic Lagrangian, G is the kinetic energy obtained from the integration of the Lagrangian of the kinetic energy density distribution, K is the kinetic energy obtained from the integration of the Hamiltonian of the kinetic energy density distribution, EG and EK are atomic energies deduced from G and K and corrected by the virial ratio, VENEO is the atomic value of the nucleus-electron potential energy, and VENEOC is its correction by the virial ratio [41,11].

The values reported here represent the final characterization of the hydrides studied and confirm the importance of the topology in the definition of the atomic structural details of the crystal around the basins characterizing each atom.

Table 7 yields interesting results with respect to the net charge of each basin, with the Mg basins being negatively charged and the H basins positively so. Unlike in the H basin, there seemed to exist a relationship between the basin volume and the net negative charge of Mg.

Table 7 yields interesting results with respect to the net charge of each basin, with the Mg basins being negatively charged and the H basins positively so. Unlike in the H basin, there seemed to exist a relationship between the basin volume and the net negative charge of Mg.

pISSN: 0255-6952 | eISSN: 2244-7113
Rev. LatinAm. Metal. Mat. 2023; **43** (2): 95-115

Table 7. Populations and atomic energies in atomic units of the hydrides under study.

Property	α-MgH_2		β-MgH_2	
	Mg	H	Mg	H
N	12.25967	0.87776	12.07050	0.96321
Q	-0.259674	0.12224	-0.070500	0.03679
L	-0.381375	0.197371	-0.437979	0.228038
G	199.65848	0.360467	199.55732	0.390939
K	199.27711	0.557838	199.11934	0.618977
EG	-200.0164	-0.36111	-199.9390	-0.39169
EK	-199.6343	-0.55884	-199.5002	-0.62016
VENEO	-481.0291	-1.06596	-480.0330	-1.17013
VENEOC	-481.4603	-1.06691	-480.4921	-1.17124
VTOT	131.0483	33.82242	121.2522	27.60927

3.3.4. Isosurfaces of the charge density and its Laplacian

Through TOPOND's graphical tools, CRYSTAL17 generated 3D scalar functions files of the premium cell of the hydrides under study. PL3D prepared these files for visualization; and CRYSPLOT, via its volumetric data section, allowed them to be visualized using jmol. Unlike those making traditional presentations, who locate scalar functions on a plane of the unit cell, we plotted fixed 3D isosurfaces with a cutoff scalar value function of 0.02 in the space of the primitive cell under study.

Figure 8 represents isosurface sequences of the charge density, the gradient, and the Laplacian for

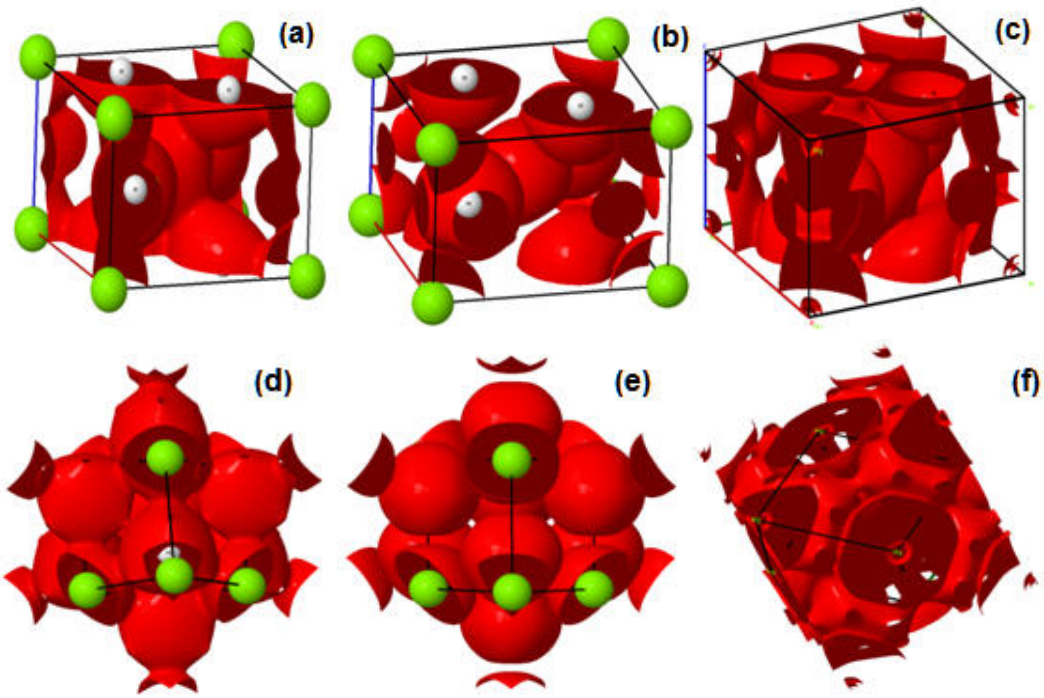

Figure 8. *Isosurfaces of the electron charge density (a, d), gradient and Laplacian of the electron charge density (c, f), taking in each case a cutoff value of 0.02 a.u. (a. b. c): α-MgH_2. (d,e,f): β-MgH_2. White ball: H. Green ball: Mg*

pISSN: 0255-6952 | eISSN: 2244-7113
Rev. LatinAm. Metal. Mat. 2023; **43** (2): 95-115

both hydrides. The left figure reflects the electron charge density distribution around the H and Mg atoms and its influx at different regions of lower density associated to the BCPs. In the center figure, the density gradient isolates the atomic domes defining unconnected spacings around each atom, while the figure associated with the Laplacian, on the right, shows the electron shell structure around the atoms. The layer structure on the isosurface of the Laplacian shown corresponds to the Mg electron layers at the corners of the lattice.

The results presented here have been checked with other basis sets, corroborating their dependence on them, this effect being magnified in scalar functions involving higher-order derivatives.

4. CONCLUSIONES

We conducted an *ab initio* study of different properties of magnesium hydrides, namely, α-tetragonal and β-cubic FCC, by means of CRYSTAL17 software using basis sets Mg_pob-TZVP_rev2, and H_pob-TZVP_rev2, and came to the following conclusions:

- The α-hydride showed an insulating character with an indirect energy band gap of 3.9651 eV discrepant with in situ ellipsometry and spectrophotometry measurements. The β-hydride, on the other hand, showed a conducting character.
- COOP and COHP analyses reflected, for both hydrides, a bonding state between the Mg-H and Mg-Mg orbitals, whereas an antibonding state was established between H-H orbitals. ICOOP showed a higher order bond in the cubic structure than in the tetragonal one. As for the antibonding energy, ICOHP portrayed the β-MgH_2 hydride as being more unstable than α-MgH_2, in agreement with the tenet held to be true by the literature.
- The bond lengths obtained from the relaxed structures of both hydrides and determined in the charge density topology study for Mg-H and H-H showed excellent agreement with those reported in the literature, with the Mg-H bond being stronger than the H-H bond in each hydride.
- The Laplacian topology of the charge density showed a charge concentration around magnesium, i.e., a higher positive charge density around Mg and a charge depletion around hydrogen, i.e., a lower charge density in both hydrides (see Tables 5 and 6).
- The topology of the charge density Laplacian and of all scalar functions involving such Laplacian evinced the distribution of electron layers around their respective atomic nuclei, corroborated by the 3D isosurfaces of these scalar functions. ELF corroborated such behavior with a maximum in a broad basin around H and a layered distribution around Mg.
- The topological vision of the atom through the conceptualization of atomic basins was ratified through the evaluation of average properties in these basins, thus generating the expected value of electron population for each atom and its deviation from the value of this charge relative to the isolated atom, this deviation thus being basis set-dependent.
- The bonding character defined by the sign of the contributions of g(r), v(r), h(r), and the Laplacian on the respective bond critical point is, in general, Closed-Shell Transition Zone, this behavior being different from that reported in our previous work using WIEN2K18.

5. AGRADECIMIENTOS

We thank Carlos Mota for reviewing this manuscript, and the group of metals physics (GFM) of the Universidad de Oriente, Cumaná, Venezuela for their continuous support.

6. REFERENCIAS

[1]. Graetz J. ISRN Materials Science. 2012. https://doi.org/10.5402/2012/863025.

[2]. Leiva DR, Jorge AM, Ishikawa Jr.T.T, Botta WJ. Mat. Trans. 2019; 60: 1561-1570.

[3]. Yartys A, Lototskyy MV, Akiba E, Albert R, Antonov VE, Ares JR, Baricco M, Bourgeois N, Buckley CE, Bellosta von Colbe JM, Crivello J.C, Cuevas F, Denys RV, Dornheim M, Felderhoff M, Grant DM, Hauback BC, Humphries TD, Jacob I, Jensen PE, de Jongh JM, Joubert MA, Kuzovnikov M, Latroche M, Paskevicius L, Pasquini TR, Popilevsky L, Skripnyuk VM, Rabkin E, Sofianos MV, Stuart A, Walker G, Wang H, Webb CJ, Zhu M. Int. J. Hydrog. Energy. 2019; 44, 7809-7859. https://doi.org/10.1016 /j.ijhydene.2018.12.212.

[4]. Wiedner ES, Chambers MB, Pitman CL, Morris Bullock R, Miller AJ, Appel AM. Chem. Rev.

pISSN: 0255-6952 | eISSN: 2244-7113
Rev. LatinAm. Metal. Mat. 2023; **43** (2): 95-115

2016; 116, 8655−8692. https://doi.org/10.1021/acs.chemrev.6b00168

[5]. Hirscher M, Yartys VA, Baricco M, Bellosta von Colbe J, Blanchard D, Bowman RC, Broom DP, Buckley CE, Chang F, Chen P, Whan Cho Y, Crivello J-Cl, Cuevas F, David WIF, de Jongh PE, Denys RV, Dornheim M, Felderhoff M, Filinchuk Y, Froudakis GE, Grant DM, MacA Gray E, Hauback BC, He T, Humphries TD, Jensen TR, Kim S, Kojima Y, Latroche M, Li H-We, Lototskyy MV, Makepeace JW, Møller KT, Naheed L, Ngene P, Noréus D, Moe Nygård M, Orimo S-i, Paskevicius M, Pasquini L, Ravnsbæk DB, Sofianos MV, Udovic TJ, Vegge T, Walker GS, Webb CJ, Weidenthaler C, Zlotea C. J. Alloy Compd. 2020; 827: 153548 https://doi.org/10.1016/j.jallcom.2019.153548.

[6]. Baran A, Polański M. Materials. 2020; 13(18): 3993. https://doi.org/10.3390/ma13183993.

[7]. Cabo M, Garrroni S, Pellicer E, Milanese C, Girella A, Marini A, Rossinyol E, Surinach S, Dolors Baro M. Int. J. Hydrog. Energy. 2011; 36: 5400-5410. https://doi.org/:10.1016/J.IJHYDENE.2011.02.038.

[8]. Kurko S, Matovic L, Novakovic N, Matovic B, Jovanovic Z, Paskas Mamula B, Novakovic J. Int.J. Hydrog. Energy. 2011; 36:1184-1189 .https://doi.org/10.1016 /j.ijhydene.2010.06.091.

[9]. Luiggi NJ. J. Phys. Chem. Solids. 2019; 131, 196-212. https://doi.org/10.1016/j.jpcs.2019.03.032.

[10]. Luiggi NJ. Mat. Today Comm. 2021; 28(18): 102639. https://doi.org/10.1016/ j.mtcomm. 2021. 102639.

[11]. Gervasio G, Bianchi R, Marabello D. Chem. Phys. Lett. 2004; 387, 481–484. https://doi.org/ 10.1016 /j.cplett.2004.02.043.

[12]. Espinosa E, Alkorta I, Elguero J, Molins E. J. Chem. Phys. 2002; 117, 5529-5542. https:// /doi:10.1063/1.1501133.

[13]. Gatti C. Chemical Bonding in Crystals: New Directions, Zeitschrift Fur Kristallographie. 2005; 220, 399-457. https://doi.org/10.1524/zkri.220.5.399.65073.

[14]. Dovesi R, Erba A, Orlando R, Zicovich-Wilson CM, Civalleri B, Maschio L, Rerat MR, Casassa S, Baima J, Salustro S, Kirtman B. WIREs Comput. Mol. Sci. 2018; 8(39): 1360. https://doi.org/10.1002/wcms.1360.

[15]. Perdew JP, Ruzsinszky A, Csonka GI, Vydrov OA, Scuseria GE, Constantin LA, Zhou X, Burke K. Phys. Rev. Lett. 2008; 100:136406 https://doi.org/10.1103/ PhysRevLett.100.136406.

[16]. Perdew JP, Burke K, Ernzerhof M.. Phys. Rev. Lett. 1996; 77: 3865-3868. https://doi.org/ 10.1103/PhysRevLett. 77.3865.

[17]. Oliveira DV, Peintinger MF, Laun J, Bredow T. J Comput Chem. 2019; 40(27): 2364-2376. https://doi.org/ 10.1002/jcc.26013.

[18]. Bortz M, Bertheville B, Bottger G, Yvon K. J. Alloy Compound. 1999; 287, L4–L6. https:// doi.org/10.1016/S0925-8388(99)00028-6.

[19]. Er S. van Setten MJ, De Wijs GA., Brocks G. J. Phys.: Condens. Matter. 2010; https://doi.org/ 10.1088/0953-8984/22/7/07420.

[20]. Available in https://legacy.materialsproject.org/materials/mp-23710 (1008901)

[21]. Available in https://discover.materialscloud.org/topomat/materials/5437 (5438)

[22]. Schlegel HB. Theor. Chim. Acta. 1984; 66, 333-340. https://doi.org/10.1007/BF00554788.

[23]. Isidorsson J, Giebels I, Arwin H, Griessen R. Phys. Rev. B. 2003; 68(11): 115112 https://doi.org/ 10.1103/PhysRevB.68.115112.

[24]. Araújo M, Lebègue S, Eriksson O, Alouani M, Ahuja B. J. Applied Physics. 2005; 98 (9): 096106 https://doi.org/10.1063/1.2128041.

[25]. Ruggiero MT, Erba A, Orlando R, Korter TM. Phys. Chem. Chem. Phys. 2015; 17 : 31023-31029. https://doi.org/10.1039/c5cp05554g.

[26]. Hughbanks T, Hoffmann R. J. Am. Chem. Soc. 1983; 105 (11): 3528-3537. https://doi.org/10.1021/JA00349A027.

[27]. Steinberg S, Dronskowski R. Crystals. 2018; 8(5): 225. https://doi.org/10.3390/cryst8050225.

[28]. Grechnev A, Ahuja R, Eriksson O. J. Phys.: Condens. Matter. 2003; 15: 7751–7776. https://doi.org/10.1088/0953-8984/15/45/014

[29]. Bader RFW. Atoms in Molecules - A Quantum Theory, vol. 22 of International Series of Monographs in Chemistry. Oxford, UK: Oxford University Press. 1990.

[30]. Lobo N , Takasaki A , Mineo K, Klimkowicz A , Goc K. Int. J. Hydrog. Energy. 2019; 44 (55): 29179-29188

[31]. Bader RFW.: Atoms in molecules. A quantum theory, Oxford University Press Inc., New York .1995.

[32]. Lepetit Ch, Fau P, Fajerwerg KM, Kahn L, Silvi, B. Coord. Chem. Rev. 2017; 345, 150-181..

[33]. Popelier PLA. Coord. Chem. Rev. 2000; 197, 169–189. https://doi.org/10.1016/S0010-8545 (99)00189-7.

[34]. Aray Y, Rodrıguez, J, Lopez-Boada R. J. Phys. Chem. A. 1997; 101: 2178 - 21218. https://doi.org/10.1021/JP962390A

[35]. Cremer D, Kraka E Angew. Chem. Int. Ed. 1984; 23:627–628. https://doi.org/10.1002/anie.198406271.

[36]. Cremer D, Kraka E. Croat. Chem. Acta. 1983; 57, 1259–1281.

[37]. Gatti C, Saunders VR, Roetti C. J. Chem. Phys. 1994;101:10686-10696. https://doi.org/10.1063/1.467882.

[38]. Gatti C, Casassa S. TOPOND14 User's Manual, CNR-ISTM of Milano, Milano. http://crystal.unito.it/topond.php. 2013.

[39]. Popelier PL.A. Chem. Phys. Lett. 1994; 228: 160-164. https://doi.org/10.1016/0009-2614(94)00897-3.

[40]. Gatti C. Acta Crystall. 1996; A52: C555.

[41]. Bader RFW, Beddall PM. J. Chem. Phys. 1972; 56: 3320-3329. https://doi.org/10.1063/1.1677699.

pISSN: 0255-6952 | eISSN: 2244-7113
Rev. LatinAm. Metal. Mat. 2023; **43** (2): 95-115

7. MINIBIOGRAFÍA DE AUTORES

NEY-LUIGGI Dr. en Metalurgia Física (Grenoble INP, Francia). MSc. en Metalurgia Física (Grenoble INP, Francia). Licenciado en Física (UDO-Venezuela). Profesor Titular del Departamento de Física de la Universidad de Oriente (UDO-Venezuela), con experiencia en caracterización experimental y teórica de metales y aleaciones (Propiedades eléctricas, termoeléctricas, estructurales, elásticas evaluadas por DFT, simulación de transformaciones de fases por métodos estocásticos y clásicos, síntesis por aleación mecánica de aleaciones de Al, Mg y Fe). (ORCID: 0000-0002-0215-1318).

pISSN: 0255-6952 | eISSN: 2244-7113
Rev. LatinAm. Metal. Mat. 2023; **43** (2): 95-115